Aust. J. Phys., 1990, **43**, 601–15

The Study of Surfaces Using Ion Beams*

D. J. O'Connor, B. V. King, R. J. MacDonald, Y. G. Shen and Xu Chen

Department of Physics, University of Newcastle,
Newcastle, N.S.W. 2308, Australia.

Abstract

The study of surfaces has progressed by the development of techniques which use different probing species in the form of electrons, ions and photons. Specialisation within the use of each probe has resulted in the subsequent development of methods of analysis tuned to obtain specific information about a surface. In this presentation the various uses of ion scattering spectrometry over a wide range of energies will be reviewed to illustrate how it has been successfully used to yield structural and compositional information of the surface atomic layer and the near surface region.

1. Introduction

Ion scattering spectrometry (ISS) is a powerful multi-facetted tool for structural and compositional analysis of a surface over a range of depths from the surface atomic layer itself down to a micron. The great strengths of the technique are that the measurements are made in real space rather than reciprocal space as is the case for structural electron spectroscopies and most of the derived information can be extracted with the aid of relatively unsophisticated computer models. The general term ISS covers a wide range of incident energies and both the nature of the analysis and the accessible information changes as the energy increases. These can be generally subdivided into the following.

(a) Low energy ion scattering (0·1–10 keV). An inherently surface sensitive technique which usually involves the use of inert gas or alkali ions incident on the surface and the detection of scattered ions. The surface selectivity results from the combined effects of scattering cross section and charge exchange. The large scattering cross section at low energies minimises the fraction of projectiles entering the solid and the charge exchange process ensures that projectiles which do penetrate are efficiently neutralised resulting in negligible ion yield from the subsurface region.

(b) Medium energy ion scattering (20–200 keV). In this approach to surface analysis either H^+ or He^+ are the usual projectiles and electrostatic (or less commonly solid state) energy analysers detect the scattered projectiles. The

* Paper presented at the Workshop on Interfaces in Molecular, Electron and Surface Physics, held at Fremantle, Australia, 4–7 February 1990.

0004-9506/90/040601$03.00

cross section for scattering is considerably smaller than for LEIS and the ions have a high probability of penetrating deep into the solid. The charge exchange process is less critical at these energies and the charge fraction (which is typically 0·5 to 0·95) can easily be measured. This application of ISS utilises channelling and blocking geometries to determine surface interlayer spacing relaxations for clean and adsorbate surfaces and the structure of near-surface interfaces (Van der Veen 1985).

(c) Rutherford backscattering spectrometry (>0·5 MeV). At these energies the solid is transparent to depths of typically 1 micron and the solid state detector used to measure the energy spectra is unaffected by the charge state of the scattered particles. This is a well documented and routine method of analysis which will not be considered in this review. The reader is referred to Chu *et al.* (1978) for a comprehensive description of the application of RBS to surface analysis problems.

In this review of the use of ion beams in surface analysis the general principles will first be outlined and then four case studies highlighting different aspects of LEIS and MEIS will be presented. More detailed descriptions of the application of ISS are to be found in the literature (Bird and Williams 1989).

In all cases under consideration, the projectile energies are sufficiently high that the collisions can be treated as classical elastic binary processes. As a consequence of the elastic nature of the scattering event the energy of a scattered particle E_1 detected at an angle θ is independent of the interaction potential, and is a function only of the incident energy E_0, θ and the ion and target masses M_1 and M_2:

$$\frac{E_1}{E_0} = \left(\frac{\cos\theta + (\mu^2 - \sin^2\theta)^{\frac{1}{2}}}{1+\mu} \right)^2, \tag{1}$$

where $\mu = M_2/M_1$, and for the recoil particle by

$$\frac{E_2}{E_0} = \frac{4\mu}{(1+\mu)^2} \cos^2\phi, \tag{2}$$

where ϕ is the recoil angle.

The yield of scattered particles is related to the concentration of target atoms by the expression

$$Y = N_i N_a \sigma(E_0, \theta)\, T(E) \Delta\Omega, \tag{3}$$

where N_a is the number of surface atoms of type A per unit area and N_i is the number of incident particles. For convenience the term $\sigma(E_0, \theta)$ has been used as a short-hand represention for the differential scattering cross section $d\sigma(E_0, \theta)/d\Omega$ for scattering of ions of energy E_0 through the angle θ and $T(E)$ is the detection or transmission function of the energy analyser. The role of the repulsive scattering potential is represented by $d\sigma(E_0, \theta)/d\Omega$ which can be calculated if the appropriate potential is known.

2. The Scattering Cross Section

The differential scattering cross section depends on the incident ion energy, the scattering angle and the potential governing the interaction between the incident ion and surface atom. At the energies used in ISS only the repulsive part of the interatomic potential is significant and it can be represented by one form of the screened Coulomb potential:

$$V(r) = \frac{Z_1 Z_2 e^2}{r} \Phi(r/a), \tag{4}$$

where r is the interatomic spacing, Z_1 and Z_2 are the atomic numbers of the collision partners and a is the screening radius (Torrens 1972). For low energy ion–atom interactions, the Moliere (1947) representation of the Thomas–Fermi screening function is normally used as a first approximation. For this potential the screening function is given by

$$\Phi(x) = 0 \cdot 35 \exp(-0 \cdot 3x) + 0 \cdot 55 \exp(-1 \cdot 2x) + 0 \cdot 1 \exp(-6x),$$

where $x = r/a$ and the sceening radius is usually taken to be a function of the form:

$$a = \frac{0 \cdot 88534 a_0}{(\sqrt{Z_1} + \sqrt{Z_2})^{\frac{2}{3}}}. \tag{5}$$

However, this is often multiplied by a numerical factor to match the Moliere to more complex, but more accurate potentials. O'Connor and Biersack (1986) discussed one such fitting factor, however they also identified the 'Universal' potential (Biersack and Ziegler 1982) as the most accurate in ion scattering applications. The expressions for the screening radius and the screening function for this potential are

$$a = \frac{0 \cdot 88534 a_0}{Z_1^{0 \cdot 23} + Z_2^{0 \cdot 23}}, \tag{6}$$

$$\Phi(x) = 0 \cdot 1818 \exp(-3 \cdot 2x) + 0 \cdot 5099 \exp(-0 \cdot 9423x) + 0 \cdot 2802 \exp(-0 \cdot 4029x) + 0 \cdot 02817 \exp(-0 \cdot 2016x). \tag{7}$$

Although a simple analytical expression for the cross section does not exist at the energies associated with LEIS and MEIS a number of general rules apply: The differential scattering cross section increases with (i) increasing atomic number of the projectile or target (Z_1,Z_2); (ii) decreasing energy of the incident projectile; and (iii) decreasing scattering angle.

3. Shadow Cone

The shadow cone is used at all energies to obtain structural information concerning the surface and near-surface region. To explain its use it is first necessary to understand the concept of a shadow cone in ion scattering. If a projectile is incident upon a target atom (which we will assume has

a greater mass than the projectile) and it strikes 'head on', i.e. with zero impact parameter, then it will be scattered straight back along its incident trajectory. (The impact parameter is the perpendicular distance between the initial undeviated trajectory and the initial target position.) If instead it is incident with a small impact parameter it will be scattered through a large angle, and as the impact parameter becomes larger the scattering angle becomes smaller. Behind the target atom there is a shadowed region, or excluded zone (see Fig. 1) into which no projectiles can penetrate and this region is called the shadow cone. Oen (1983) derived an expression for the shape of the shadow cone based on the Moliere interatomic potential. The shadow cone radius will in general increase with increasing atomic number of the collision partners and with decreasing projectile energy. The flux at the edge of the shadow cone is enhanced over the incident ion flux as most scattered projectiles pass close to the edge of the cone. By suitable choice of geometry this shadow cone can be used to locate atoms above, in and below the surface layer. This technique has been applied (Aono *et al.* 1982, 1983; Moller *et al.* 1986; Niehus 1986; Souda *et al.* 1983) using scattered inert gas ions, scattered alkali ions and scattered neutrals with equal success in the different applications.

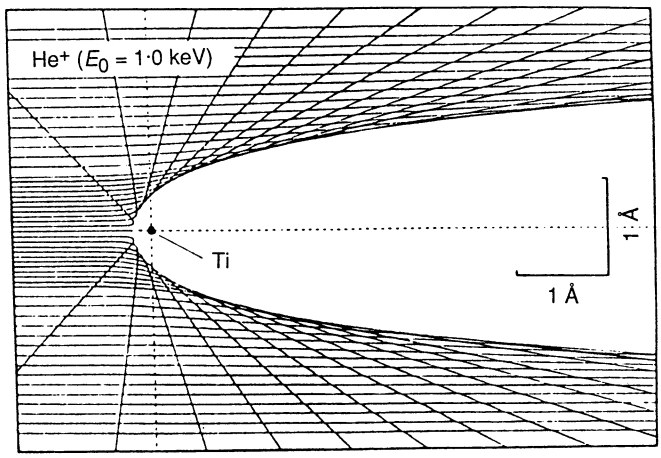

Fig. 1. Shadow cone behind a target atom created by the repulsive interaction between the projectile and the target atom.

4. Low Energy Ion Scattering

There is an important difference between the charge exchange processes experienced by inert gas ions and alkali ions near surfaces which results from their significantly different ionisation potentials. Only 1–10% of the inert gas ions scattered from the surface atomic layer will escape in the charged state and virtually all those scattered from below the surface will be neutrals. When alkali ions are incident upon a surface the charge fraction is not a strong function of the trajectory and consequently similar charge fractions (50–99%) are observed for both the surface and the subsurface layers. Thus alkali ions and inert gas ions can be used to yield complementary information about the surface composition. A similar benefit can be achieved if the neutral scattered

inert gas projectiles are detected (usually by time of flight techniques). The analysis of the surface composition of Ni_3Al will be used to demonstrate the application of some of these approaches.

Ni_3Al

The intermetallic Ni_3Al possesses two particularly attractive properties of technological interest. The first is that, unlike most materials, the yield strength of this alloy increases with increasing temperature and the second is that it has excellent corrosion resistance at high temperature. Several studies have revealed that the oxidation process involves a segregation of the Al to the surface where an amorphous AlO layer is formed. It will be shown in this example how LEIS can be used to extract basic compositional information concerning the surface while minimising the complications introduced by the charge exchange process.

The relationship between scattered ion yield and target composition for LEIS takes the form

$$Y = N_i N_a \sigma(E_0, \theta) P^+(v_\perp) T(E) \Delta\Omega , \tag{8}$$

where $P^+(v_\perp)$ is the probability that a projectile will remain in a charged state and hence be detected by electrostatic analysers. Experiments to date have identified that the principal factor in determining P^+ is the time spent near the surface and this is represented by the perpendicular component of velocity factor, $v_\perp$. Besides the uncertainty introduced by the fact that P^+ cannot be predicted with any certainty at this stage, any major surface compositional changes (e.g. oxidation) may affect the magnitude of P^+. Several methods have been developed to overcome the uncertainty introduced by the charge fraction term. For cases where the change in relative concentrations is needed or where the charge fraction is expected to change significantly (e.g. for O adsorption) the use of concentration ratios minimises the effect of the charge fraction term as it appears in the denominator and the numerator:

$$Y_a/Y_b = (N_a/N_b)(\sigma_a/\sigma_b)(P_a^+/P_b^+) . \tag{9}$$

Another approach used in the analysis of clean and adsorbate covered surfaces is to calibrate all the terms in equation (8) with clean surface standards of each component and use these as references. The assumption behind this approach is that the ion fraction is principally dependent on the primary collision partner rather than the average surface composition. This method has been successfully applied to a variety of surfaces.

The surface structure of $Ni_3Al(001)$ has been shown (Sondericker *et al.* 1986) to have an ordered equal mix of Ni and Al atoms in the outermost atomic layer and a pure Ni layer below. This can be tested by comparing the yields for He and Li scattered off this surface. Two geometries have been chosen for this analysis. When the ion beam is incident at 45° to the surface along the [100] surface direction the surface atoms shadow the second layer, so for both types of projectiles only yield from the surface will be observed. When the beam is incident at 35° to the surface along the [110] direction the second

layer is visible and projectiles will be scattered from it, though a significant increase in ion yield should only be observed when alkali ions are used as the inert gas ions are efficiently neutralised inside the surface.

In the absence of charge exchange the ratio N_{Ni}/N_{Al} for the [100], 45° direction should be 1·0 and for the [110], 35° should be 3·0. From Table 1 it can be observed that for the inert gas ions the ratio increases by only 7% rather than 200%, indicating how insensitive the inert gas ions are to the second layer. For the alkali ions the ratio increases significantly demonstrating the sensitivity to the subsurface layers, however it does not reach the ideal indicating that there is still some trajectory dependent neutralisation for these alkali projectiles. To make a more accurate determination of the concentration ratio a reference standard would have to be used.

Table 1. Analysis of the relative composition for $Ni_3Al(100)$ using 2 keV He and Li

Here the direction [100], 45° indicates that the ion beam was incident at 45° to the [100] surface direction. All measurements were taken at a scattering angle of 90° and have been normalised for equal beam charge. For the [100] geometry only the surface layer is visible to the incident ion beam and the analyser while for the [110] geometry both the surface and second layer are visible

Projectile	Direction	Y_{Al}	Y_{Ni}	Y_{Ni}/Y_{Al}	N_{Ni}/N_{Al}[A]
σ_{calc}(He) (pm^2 sr^{-1})		28·3	70·7		
He	[100], 45°	1048	2156	2·06	0·83
He	[110], 35°	1028	2285	2·22	0·89
σ_{calc}(Li) (pm^2 sr^{-1})		43·9	104·5		
Li	[100], 45°	57350	128100	2·23	0·94
Li	[110], 35°	66350	362400	5·25	2·20
Ideal	[100], 45°				1·00
Ideal	[110], 35°				3·00

[A] These ratios are not corrected for charge fraction.

The stability of the surface composition ratio can be monitored accurately with LEIS as temperature changes do not affect the ion fraction. This simplification leads to the conclusion (Fig. 2) that the Ni/Al ratio is stable up to a target temperature of 900°C. Although an accurate measurement of the surface composition has not been made in this example the temperature dependence can nevertheless be determined precisely. In a similar application the effect on the surface composition of continuous 2 keV He bombardment is illustrated in Fig. 3 where the Ni/Al ratio change induced by preferential sputtering is demonstrated. As the sputtering proceeds the uncorrected concentration ratio (Ni/Al) rises from 1·0 to 1·6 indicating that the Al is preferentially sputtered leaving the surface Ni rich. A similar study of the oxidation of Ni_3Al has demonstrated that the adsorption of oxygen causes Al to preferentially segregate to the surface to form an AlO layer.

5. Impact Collision Ion Scattering Spectrometry (ICISS)

Perhaps the most direct use of the shadow cone and the most easily interpreted is the ICISS method developed by Aono *et al.* (1981). In this technique, and variations of it, a low energy ion beam is incident upon a

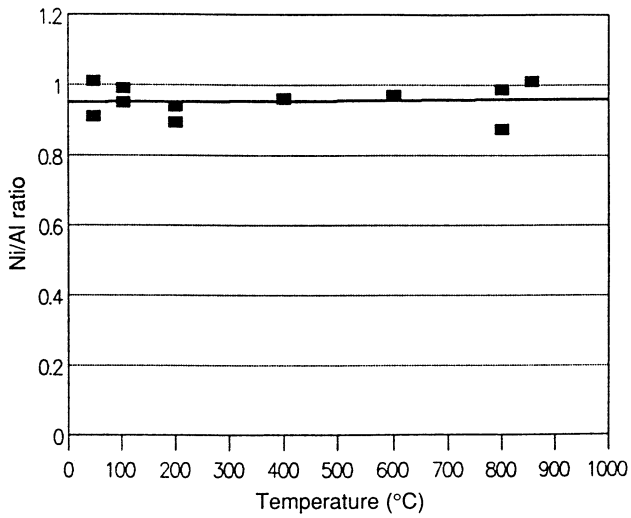

Fig. 2. Thermal stability of the Ni/Al ratio on a $Ni_3Al(001)$ surface measured with low energy ion scattering.

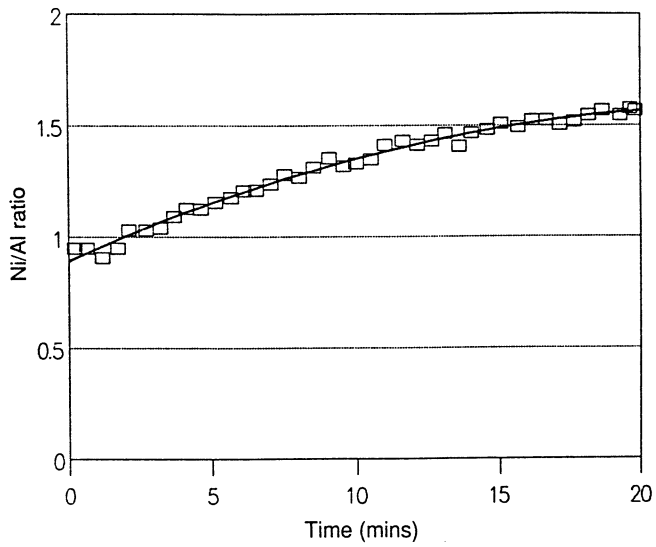

Fig. 3. Varying surface composition of $Ni_3Al(001)$ as a result of preferential sputtering of the surface by 2 keV He bombardment.

surface and the detector is placed within 30° of the 180° scattering angle. Consequently for a scattered particle to be detected it must have a near zero impact parameter collision with one of the target atoms. If an ion beam is incident at a shallow angle to a surface no scattering will be observed at 180° as each atom in the surface lies in the shadow of the preceding atom. As the angle of incidence of the ion beam is increased the shadow cone rotates about each scattering centre and at some critical angle of incidence the edge of the shadow cone will intersect the neighbouring atom. The scattered ion yield

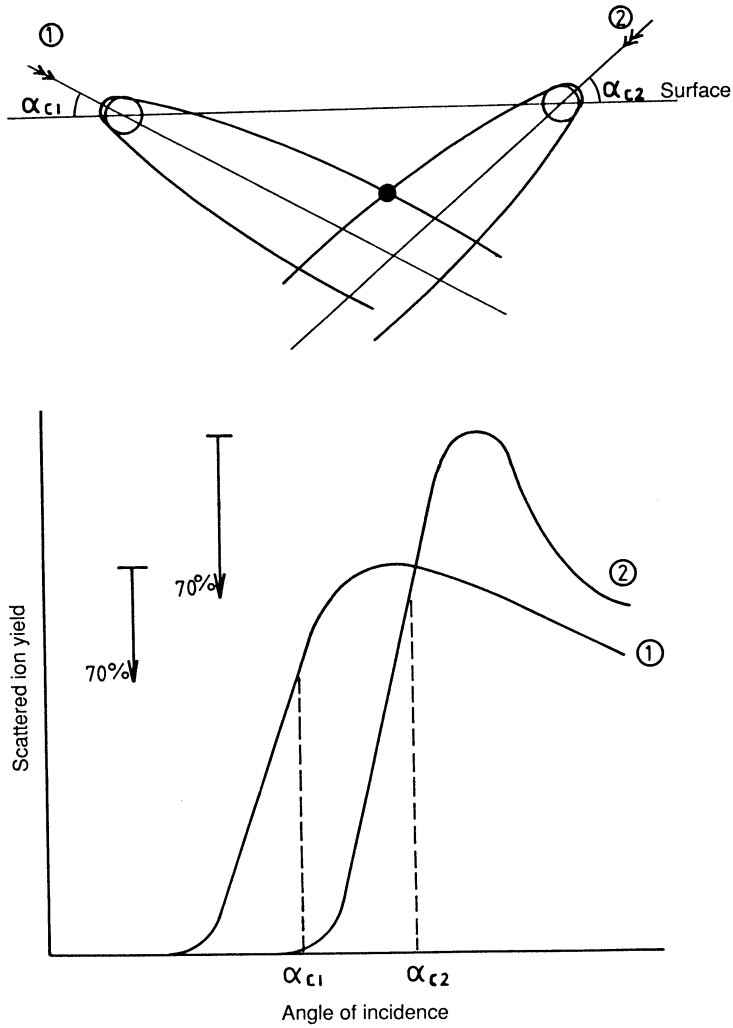

Fig. 4. Use of the shadow cone to locate atoms on or under the surface atomic layer.

will be zero below the critical angle and beyond this angle it will peak (from the flux enhancement) then fall to an intermediate value. The measurement of the interatomic spacing comes from the critical angle determination and a knowledge of the shape of the shadow cone. An early application by Aono *et al.* (1981) of this technique was the location of the carbon under the surface layer of Ti in a TiC(111) surface (Fig. 4). In this application the C was found to sit asymmetrically between the surface Ti atoms and hence there are two critical angles depending on the direction from which the ion beam is incident. The position of the C is 87±8 pm below the Ti surface layer.

One variation of this technique is coaxial impact collision ion scattering spectrometry (CAICISS) in which the scattered ion yield is detected as close to 180° as physically possible (typically >175°). The main advantages of this technique are:

(1) Quantitative structural analysis of solid surfaces can be made easily.
(2) Up to about 10 layers below the surface can be seen when using neutral scattered projectiles. This makes the technique very useful for analysing epitaxial growth of thin films.
(3) Layer-by-layer elemental analysis over several atomic layers is possible.
(4) A surface-sensitive mode or a bulk-sensitive mode can be selected by measuring the reflected ions or neutrals respectively.
(5) Information on chemical states (charge states) of surface atoms can be obtained
(6) CAICISS is convenient for monitoring various surface processes *in situ* as the ion dose needed for analysis is of the order of 1 nC.
(7) CAICISS is suitable for the time-resolved analysis of dynamical processes at surfaces.

The dual sensitivity of CAICISS to surface and subsurface structure analysis (by detection of both ions and neutrals separately) is important in monitoring epitaxial growth behaviour. To demonstrate its capabilities an example involving the epitaxial growth of CaF_2 on a carefully prepared 7x7 Si(111) surface will be described.

CaF_2/Si(111)

Thin epitaxial insulators have great potential for application in silicon-on-insulator (SOI) devices, 3D integrated circuits or to lattice match III–V semiconductors onto Si substrates. CaF_2 is a favoured insulator for epitaxial growth on Si since it is lattice matched (within 0·6% of the Si lattice parameter at room temperature) and high quality films can be grown by molecular beam epitaxy on Si substrates.

CaF_2 films (1–100 monolayers thick) were deposited by molecular beam epitaxy onto a heated Si(111) substrate (between RT and 700°C) and analysed using CAICISS and LEED during or after deposition. The deposited CaF_2 films always exhibited a 1×1 LEED pattern. Ion scattering angular spectra characteristic of good epitaxial growth of CaF_2 were obtained. There are two geometrical arrangements for the growth of a thick CaF_2 on a Si substrate and these are distinguished as an A- or B-type configuration. In A-type film the CaF rows would be parallel to the diagonal rows of Si atoms while in B-type they would be reversed. For a one monolayer film the expected positions of Ca and F are shown in Fig. 5. These growth modes can be distinguished as the A-type structure would result in minima in the Ca yield (blocked by the surface F) at 13° and 158°, while for the B-type structure the minima would occur at 22° and 167°. It can be clearly seen that the experimental results (Fig. 5) support the B-type model.

Controversy also exists over the position of the Ca atom with respect to the underlying Si atom. Photoemission studies indicate that the Ca sits in the three-fold T site, whereas medium energy ion scattering results lead to a T_4 site assignment (see Fig. 6). Transmission electron microscopy results have been used to justify both models. The comparison of experimental results with a computer simulation of the ion scattering from eight layers of CaF_2 on Si reveals that the CAICISS results agree better with a T_4 site (Fig. 7).

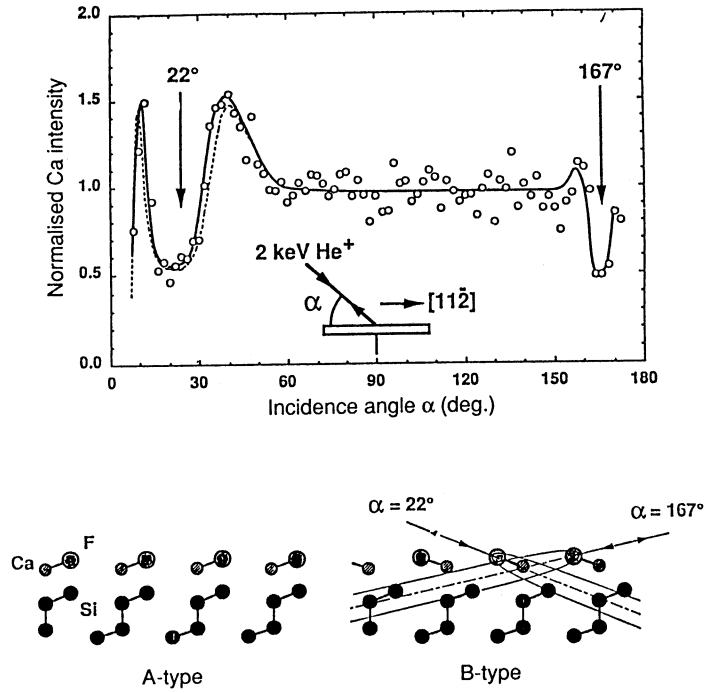

Fig. 5. The experimental determination of the structure of CaF_2 on a Si substrate. The A- and B-type structures are characterised by different characteristic shadowing angles (13° and 158° for A-type and 22° and 167° for B-type). The experimental results confirm the B-type structure.

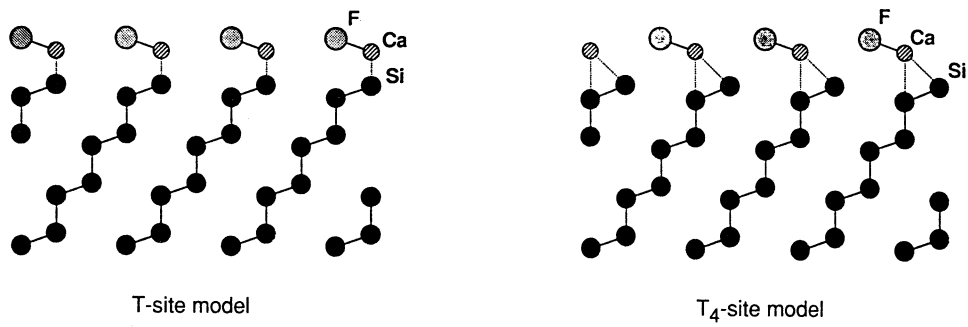

Fig. 6. Possible terminations for the CaF_2 on Si with the Ca having a different registry with the interfacial Si atoms.

This computer simulation is sufficient to yield a good estimate of the angular positions of the peaks and a rough estimate of the peak height. More detailed information on the structure of the surface and near-surface layers is possible with more detailed experiments and more sophisticated simulations.

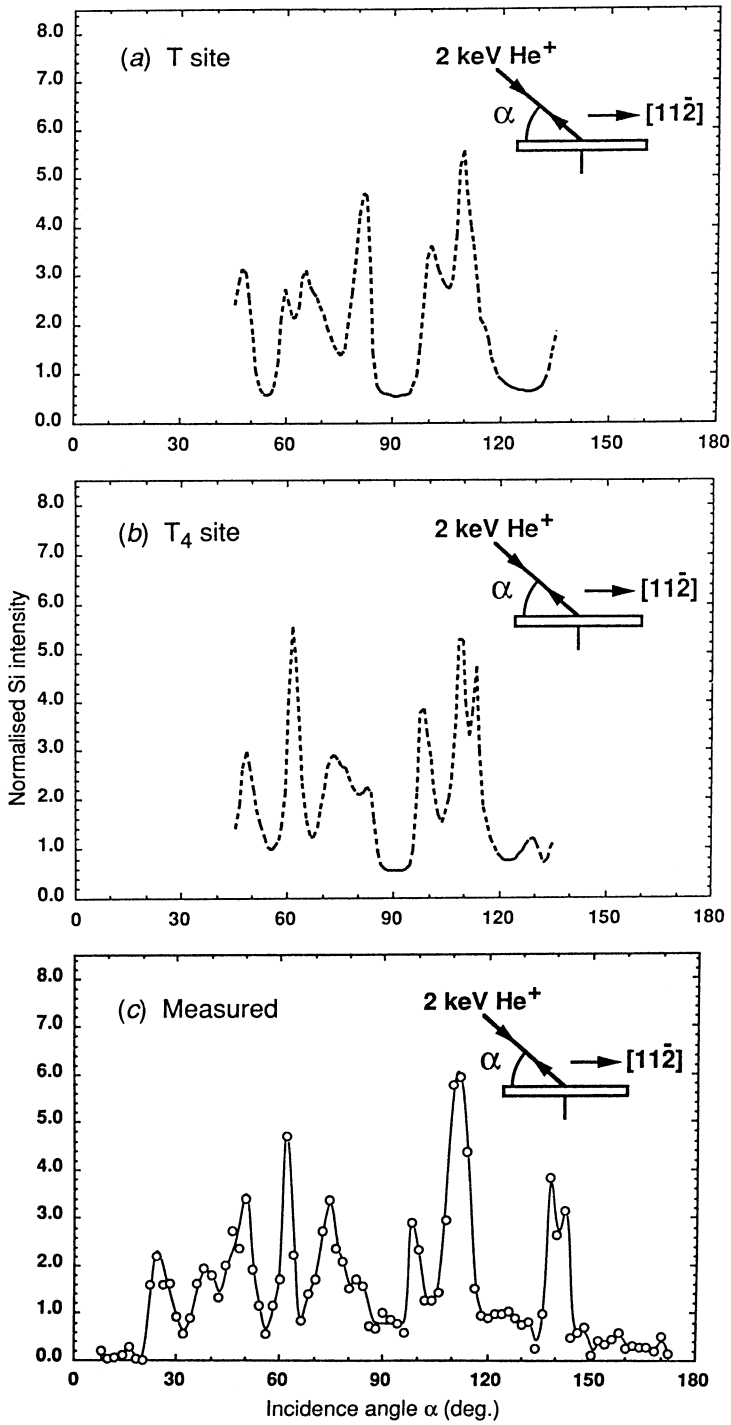

Fig. 7. Variation of the scattered yield from Si predicted by a computer model for the (*a*) T site and (*b*) T_4 site compared with (*c*) the measured yield variation. Best agreement over the range (40°–130°) is for the T_4 site.

6. Medium Energy Ion Scattering

In general medium energy H^+ ions produce a shadow cone whose radius is comparable with the thermal vibration amplitude of atoms in a solid. When an ion beam is incident upon a low index crystal direction the first atom of the string only partly shadows the second atom as they both may be off their ideal sites due to thermal vibration displacements. The sensitivity to the surface can be further improved if the detector is also aligned along a low index direction. Thus, when a subsurface atom is struck the probability of the projectile escaping to the detector is reduced as it will be scattered out of the exit direction by the atoms closer to the surface in the exit chain. Under such 'double alignment conditions' it is possible that only the top two or three atomic layers will contribute to the scattered ion yield (Van der Veen 1985). This is ideal for determining the surface relaxation and the surface reconstruction in the outermost layers of a solid. To extract the most detail from the measurements it is necessary to compare the results with a computer simulation as complete as possible. As several physical parameters may contribute to the scattered ion yield the comparison between experiment and simulation is made by a χ^2 minimisation or by an R-factor minimisation to make the final determination as objective as is possible. The parameters to be considered include

(1) composition (layer-by-layer),
(2) interlayer relaxation,
(3) surface reconstruction,
(4) enhanced thermal vibrations of the surface atoms,
(5) nature of thermal vibrations, correlated or uncorrelated,
(6) interatomic potential governing the repulsive interaction.

Table 2. Results of an MEIS analysis of the structure and composition associated with the surface segregation of a Pt in a PtNi(111) surface

	Pt (%)	Ni (%)	Total (%)	Thermal vibration enhancement
First layer	76±2	19±3	95±5	1·48±0·10
Second layer	27±3	71±3	98±6	1·21±0·10
Third layer	53±5	46±5	99±10	1·08±0·10
$\Delta D_{12} = -2 \cdot 0 \pm 0 \cdot 5\%$				
$\Delta D_{23} = -2 \cdot 0 \pm 0 \cdot 5\%$				

In a recent study by Deckers *et al.* (1990) of the PtNi(111) surface a full range of geometries was utilised to extract the most detailed information possible on the surface structure and layer-by-layer composition. By using an incident direction in which the first layer atoms largely shadowed the second and subsequent layers it was possible to measure principally the first layer. In a second geometry both the first and second layers were equally exposed to the incident beam and all deeper layers were largely shadowed. Thus, when combined with the results of the first layer it was possible to extract second layer specific information. A similar procedure was used with the third layer. It was possible to measure the surface segregation of Pt on this surface (76±2% Pt)

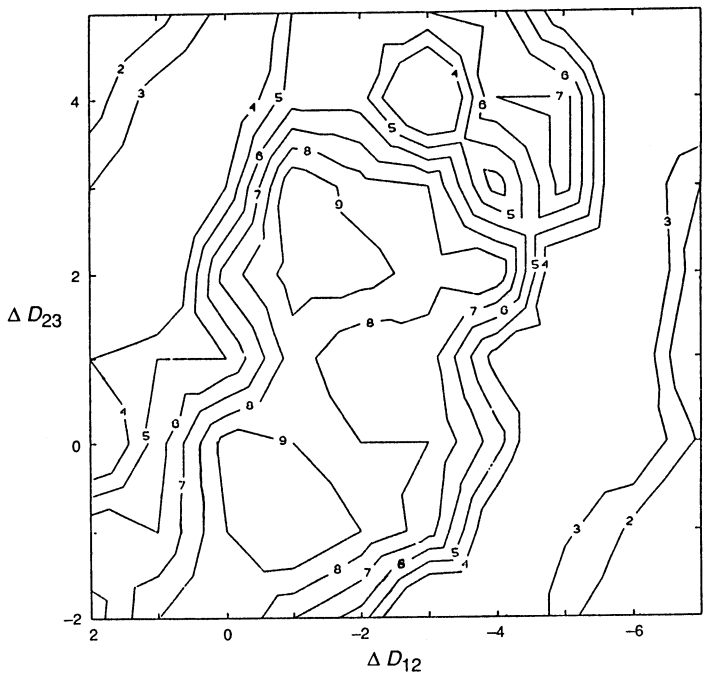

Fig. 8. An *R*-factor plot comparing the quality of fit between a computer simulation of different surface relaxations and measurements for the (110) scattering plane in a $Fe_{72}Cr_{28}$(110) surface. The existence of two clear minima are attributed to the existence of distinctly different regions on the surface which are clusters of Cr or Fe.

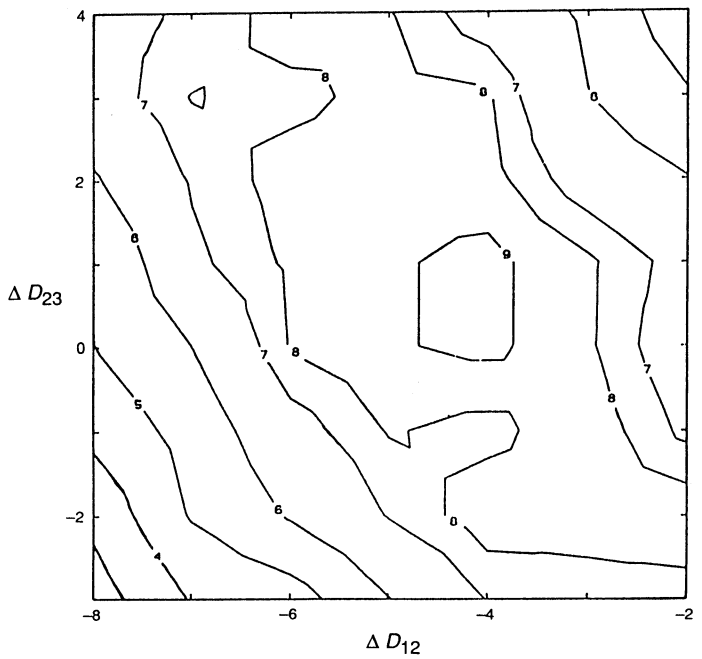

Fig. 9. By modelling the segregation and clustering of Cr on a $Fe_{72}Cr_{28}$(110) surface it has been possible to establish an estimate of the surface composition of the Cr and to determine the different relaxations experienced by the different regions. The single minimum in this *R*-factor plot arises because an offset has been introduced between the relaxations experienced by the different regions.

and observe that the second layer Pt composition (27±2% Pt) dropped to well below the bulk value. As part of the analysis the interlayer relaxations and the thermal vibration amplitudes were determined and are listed in Table 2.

The complete analysis of the PtNi was aided by the significant difference in projectile energy after the elastic scattering event. This allowed additional information concerning the Pt and Ni to be independently determined. This is not possible in cases where the target masses are similar in mass, e.g. in the case of stainless steel. Normally stainless steel is composed of Fe, Ni and Cr and it is the segregation of Cr to the surface which yields its most interesting physical and chemical properties. To study the effect of this segregation a single crystal of $Fe_{72}Cr_{28}(110)$ was analysed and the results are displayed in the *R*-factor plot in Fig. 8. This plot is a graphical representation of the comparison of the computer simulation results with the experimentally determined angular distribution of scattered particles. The *R* factor is defined by

$$R = 100\left(\frac{1}{N}\sum_{i=1}^{N}(Y_i^{\mathrm{cal}}/WY_i^{\mathrm{exp}} - 1)^2\right)^{\frac{1}{2}}, \tag{10}$$

where Y_i^{cal} are the results of a detailed computer simulation, Y_i^{exp} are the measurements and W is a weighting factor.

Table 3. Interatomic relaxations of the different regions of a $Fe_{78}Cr_{22}(110)$ surface which exhibits clustering of the surface segregated Cr and different relaxations for clusters of different composition

Element	Fe	Cr	Uncertainty
Surface composition	30%	70%	±10%
First layer relaxation	−3·5%	−2·5%	±2%
Second layer relaxation	−1%	+2%	±2%

In previous studies it was found that the Cr segregates to the surface to form a 65% Cr rich surface atomic layer and there is some clustering of the Cr. While the Fe and Cr cannot be energetically resolved the existence of two minima in the *R*-factor plot (Fig. 8) for three different scattering geometries leads to the conclusion that there are two different structures on the surface. As the stainless steel is not an ordered alloy the simulation of such an inhomogenous but ordered surface is normally difficult. In an new approach the simulation of this surface model was achieved with a simpler computer simulation than would normally be contemplated. As the mass and atomic number of Fe and Cr are similar, and the scattered ion energy are not easily distinguishable, the experimental results were compared with results obtained for a Fe surface, but with two different sets of surface relaxations added incoherently. This assumes that there are areas on the surface with one surface structure due to Cr clusters and a different surface structure where Fe predominates. After extensive analysis of various combinations of parameters it was possible to arrive at an *R*-factor plot which had only one minimum (Fig. 9) and the base level of disagreement was limited by the statistical uncertainty associated

with the experimental measurements. From this result it was concluded that the surface is composed of 70+10% Cr and the two surface relaxations are given in Table 3. The composition has a significant uncertainty as it has been determined indirectly from structural information and while the absolute accuracy on the relaxation is ±2%, the relative difference between the two surface structures has been determined to an accuracy of typically ±1%.

7. Conclusions

The examples given here are by no means exhaustive and are designed to give a general feel for the range of applications in which ISS is used to give clear surface and subsurface structural and composition analysis. For the higher energy probes the analysis is uncomplicated by secondary effects like charge exchange, while for low energy ion scattering it has been demonstrated that useful information can be obtained despite the existence of this uncertainty. The rate of progress in understanding the charge exchange mechanisms is such that in the near future there may be little uncertainty involved in the low energy ion techniques. This is not a problem when using time of flight techniques as there both ions and neutrals are detected.

References

Aono, M., Hou, Y., Oshima, C., and Ishizawa, Y. (1982). *Phys. Rev. Lett.* **49**, 567.
Aono, M., Hou, Y., Souda, R., Oshima, C., Otani, S., and Ishizawa, S. (1983). *Phys. Rev. Lett.* **50**, 1293.
Aono, M., Oshima, C., Zaima, C., Otani, S., and Ishizawa, Y. (1981). *Jap. J. Appl. Phys.* **20**, L829.
Biersack, J. P., and Ziegler, J. F. (1982). 'Springer Series in Electrophysics', Vol. 10, pp. 122–156 (Springer: Berlin).
Bird, J. R., and Williams, J. S. (1989). 'Ion Beams for Materials Analysis' (Academic: New York).
Chu, W.-K., Mayer, J.W., and Nicholet, M.-A. (1978). 'Backscattering Spectrometry' (Academic: New York).
Deckers, S., Habraken, F. H. P. M., van der Weg, W. F., van der Gon, A., Pluis, B., van der Veen, J. F., Geus, J. W., and Baudoing, R. (1990). *Phys. Rev.* (submitted).
Moliere, G. (1947). *Z. Naturforsch.* **2A**, 133.
Moller, J., Niehus, H., and Heiland, W. (1986). *Surf. Sci. Lett.* **166**, L111.
Niehus, H. (1986). *Surf. Sci. Lett.* **166**, L107.
O'Connor, D. J., and Biersack, J. P. (1986). *Nucl. Instrum. Meth.* B **15**, 14–19.
Oen, O. (1983). *Surf. Sci.* **131**, L407.
Sondericker, D., Jona, F., and Marcus, P. M. (1986). *Phys. Rev.* B **33**, 900.
Souda, R., Aono, M., Oshima, C., Otani, S., and Ishizawa, Y. (1983). *Surf. Sci. Lett.* **128**, L236.
Torrens, I. M. (1972). 'Interatomic Potentials' (Academic: New York).
Van der Veen, J. F. (1985). *Surf. Sci. Rep.* **5**, 119.

Manuscript received 9 March, accepted 6 August 1990